Krüger, F., Weber, M. (1992): The effect of low-velocity sediments on the mislocation vectors of the GRF array. - Geophysical Journal International, 108, 1, pp. 387—393.

DOI: http://doi.org/10.1111/j.1365-246X.1992.tb00866.x

Geophys. J. Int. (1992) **108**, 387–393

RESEARCH NOTE

The effect of low-velocity sediments on the mislocation vectors of the GRF array

F. Krüger and M. Weber

Seismologisches Zentralobservatorium Gräfenberg, Krankenhausstraße 1, D-8520 Erlangen, Germany

Accepted 1991 June 18. Received 1991 June 17; in original form 1991 March 25

SUMMARY

The GRF array is situated on Jurassic limestone of the Franconian Alb in SE Germany. The mislocation vectors show symmetry axes in their slowness and azimuth components. For the slowness the line of separation is at about 95° against north. The azimuth pattern shows a symmetry axis nearly perpendicular to the axis in the slowness pattern. Waves arriving from NE have a reduced slowness, whereas waves from SW have a larger slowness. The largest azimuth anomalies are found in the directions where the slowness components change direction. These effects can to a large extent be modelled by a low-velocity sedimentary layer dipping to NNE with about 0.8° dip. Such a sedimentary wedge correlates well with the geological data, is able to reproduce the observed mislocation vector pattern and explains a major part of the observed traveltime residuals. It furthermore demonstrates that local effects, like the influence of sedimentary covers, should be removed before inversion procedures and tomographic methods are applied.

Key words: mislocation vector, sediment, seismic array, site effect, tomography.

INTRODUCTION

The GRF array is situated in SE Germany and consists of 13 stations (see Fig. 1) equipped with broadband Streckeisen seismometers STS1; three of the stations are three-component stations. The maximum aperture of the array is 100 km; for details see e.g. Harjes & Hanka (1986).

Since the installation of seismic arrays, several investigations were undertaken to analyse the observed slowness and azimuth anomalies. Berteussen (1976) showed that most of the inhomogeneities at NORSAR are located in the crust. Faber, Plomerova & Babuška (1986) presented a study of mislocation vector pattern of the GRF array together with an analysis of *P*-wave traveltime residuals. They concluded that the velocity in the crust increases from north to south beneath the array. The existence of a low-velocity zone located in the upper mantle to the NE of the array was also proposed. The mislocation vector pattern is reinterpreted in this study as being to a large part produced by the sediments under the GRF array.

OBSERVATIONS

The database of the GRF array mislocation vectors consists of 276 vectors in the slowness–azimuth plane, including the 140 vectors determined by Faber *et al.* (1986), encompassing now events up to 1989. The distribution of the events is shown in Fig. 2. Slowness and azimuth were measured on WWSSN-SP filtered broadband data under the assumption of a plane wavefront propagation across the array. The theoretical values were calculated from the USGS Preliminary determination of epicentres (PDE) and with the Jeffreys–Bullen tables (Jeffreys & Bullen 1940). Fig. 3 shows the mislocation vectors.

For a better understanding the mislocation vectors are decomposed into their slowness and azimuthal components. Fig. 4(a) shows the slowness component while Fig. 4(b) shows the azimuthal component.

In the slowness plot (Fig. 4a) waves arriving with an azimuth between about 300° and 95°, i.e. waves from about WNW to about east, show a reduction in slowness with respect to the theoretical value (PDE solution). Waves arriving from 95° to 300° have an increased slowness with about the same magnitude. The line of separation at 95° is clearly defined, whereas the polarity reversal at 300° is less clear. The main feature of the slowness anomaly is a separation into two regions, i.e. reduced slowness in the north and increased slowness in the south.

The azimuth components (Fig. 4b) also show a symmetry. The line of separation is at about 10°. Changes in the

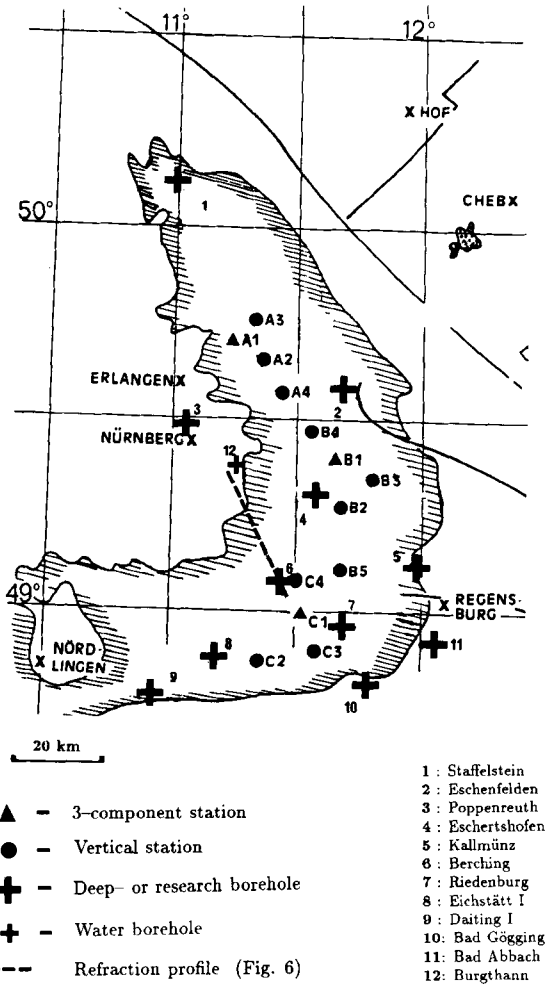

Figure 1. Location of the GRF stations (vertical and three-component) on the Franconian Jura and of boreholes (number 1 to 12) in SE Germany. Also shown is the refraction line of Bader (1982a). Solid lines indicate the main fault systems.

polarity can also be found at about 120° and less pronounced around 330° and 215° where the coverage unfortunately is not very good. The largest anomalies occur in the east at about 110° with an amount of 10° on the average and a maximum of 15°.

GEOLOGY

In the area of the GRF array several boreholes were drilled, some of them reaching the granite basement (Schmidt-Kaler 1969, 1985; Gudden 1970, 1982; Salger & Schmid 1982; Schmid 1982; Gudden & Schmid 1985). The locations of these boreholes are shown in Fig. 1.

Figure 5 shows the contour map of the top of the basement with respect to *sea-level* under the GRF array modified after Gudden & Schmid (1985, fig. 8). The southern stations are situated on the crest of the variscic basement of granite and gneiss (Dinkelsbühl-Berching high), which in this region is only 300–400 m below the surface. The basement surface is dipping to the NNE. Near Staffelstein the basement is more than 1600 m below surface (Gudden & Schmid 1985). Under the surficial Malm layer of

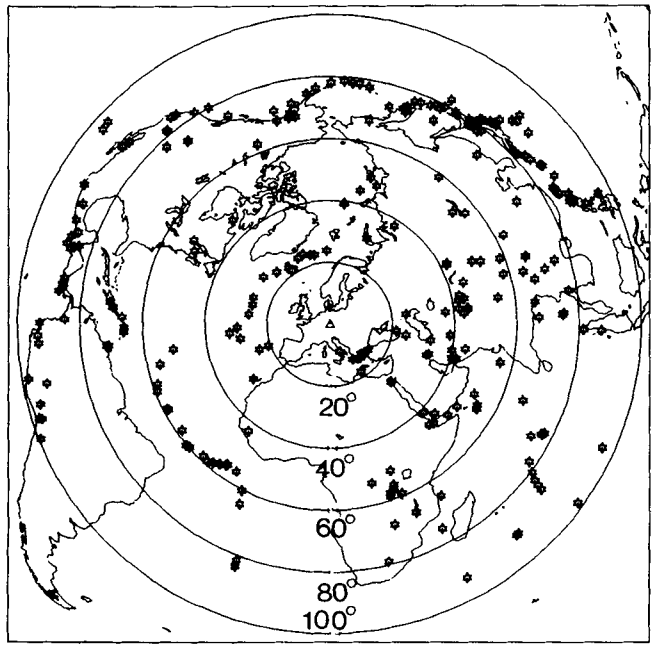

Figure 2. Distribution of the 276 events (stars) used in this study. The projection is azimuthal equidistant with GRF as the projection pole (triangle). Epicentral distances are given in degrees from station A1.

limestone with a high velocity of 5.0 km s^{-1} layers of sandy and clayish sediments with low velocities occur (Bader 1982b) with increasing thickness towards NNE under the array. Between subarray A (stations A1–A4) and subarray B (stations B1–B5) these sediments reach a thickness of 1000 m near the borehole of Eschenfelden (Bader, personal

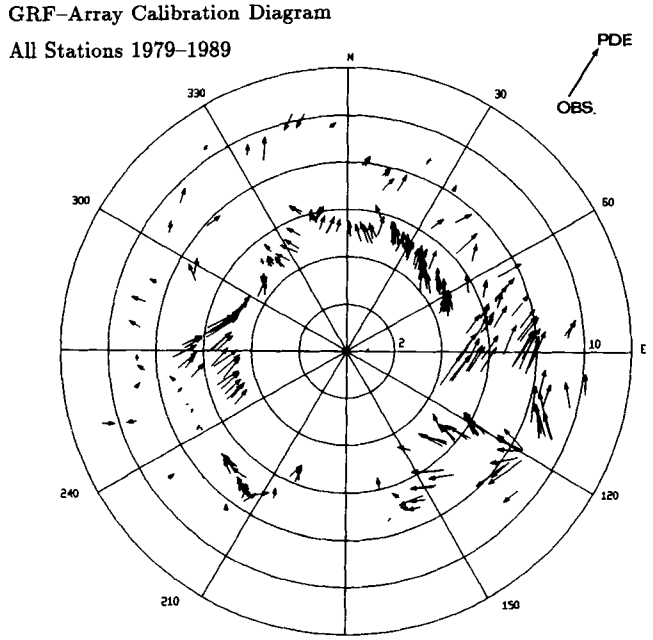

Figure 3. Mislocation vectors for the 276 events shown in Fig. 2. The grid is given radially in 2 s deg^{-1} intervals and the backazimuth in 30° intervals, respectively. The tail of an arrow is the observed and the tip is the corresponding theoretical value (PDE solution), respectively.

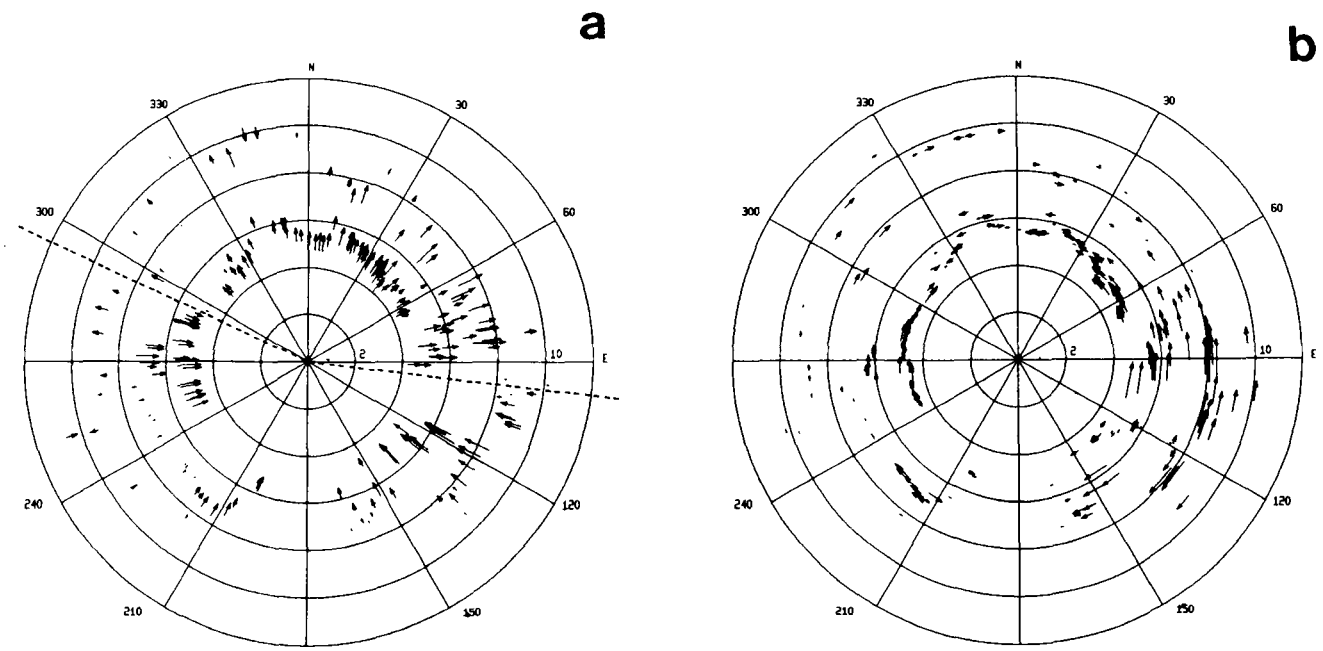

Figure 4. (a) Slowness components of the mislocation vectors of the GRF array. The line of separation is at approximately 95°. (b) Azimuth components of the mislocation vectors of the GRF array. The line of separation is at approximately 10°.

communication). North of subarray A the Buntsandstein increases in thickness and Zechstein and lower permian sediments have been drilled between Bayreuth and Staffelstein.

Bader (1982b) gives detailed *P*-wave velocities derived from refraction measurements along a profile from a point near station C1 in the direction towards Nürnberg (dashed line in Fig. 1) for Dogger, Lias and Keuper (Fig. 6).

MODELLING THE EFFECTS OF A SEDIMENTARY WEDGE

Using the information given in the previous section a model of the structure under the GRF array was constructed that consists of a sedimentary wedge between the surficial high velocity top layer of the Malm (limestone) and the top of the granite basement. Since the limestone layer is fast and rather uniform across the array and will therefore affect the traveltime delays only minimally, this surficial layer has not been included in our models. We approximated the topography of the surface of the basement by a planar interface (bottom of wedge) and kept the thickness of the sediments under the limestone below station C1 at 0.15 km.

The three parameters modified are the *P* velocity of the sediments (v_{sedi}), the *P* velocity of the granite (v_{gran}) and the dip of the wedge, i.e. the thickness of the sediments under the limestone below station A1 (d_{A1}). In the first model we use $v_{sedi} = 2.4\,km\,s^{-1}$, $v_{gran} = 5.6\,km\,s^{-1}$ and $d_{A1} = 1.0\,km$. We are interested in the size of effects the sediments can produce, therefore we also study two additional models. Since according to Stein (personal communication) the sediment velocity decreases towards W and since a v_{gran} of $5.6\,km\,s^{-1}$ might be too small our second model has values of $v_{sedi} = 2.2\,km\,s^{-1}$ and $v_{gran} = 5.8\,km\,s^{-1}$. The sediments under A1 could be up to 0.2 km thicker and Faber *et al.* (1986) suggest that the sedimentary layers in the northernmost part of the array are about 1.5 km thicker than under the southernmost stations. Therefore our third model uses $d_{A1} = 1.2\,km$ and the velocities of model 2. These two models have to be considered as extreme models.

Using a 3-D ray-tracing program rays from teleseismic sources were traced through these models and their endpoints and arrival times across the area of the array recorded and processed in analogy with the GRF data to obtain the mislocation vectors.

The result of this procedure is shown in Figs 7(a) and (b). Shown are the average values in 30° bins starting from north; see also Figs 3 and 4. The bars at the data are the standard deviations of the observations. The maximum standard deviation occurring in the models due to the use of sources at different distances is indicated at the right of the model curves. As can be seen in Figs 7(a) and (b) the sinusoidal trend of slowness and azimuth is well represented by the three models, where model 1 is a conservative representation of the local geology. Figs 8(a) and (b) give the observations corrected for the effects of the three models, i.e. the data after the removal of the effects produced by the sedimentary wedge. Whereas the uncorrected data have a standard deviation of $0.5\,s\,deg^{-1}$ in Fig. 8(a), the removal of the effects of the different models reduces the standard deviation by 38, 44 and 50 per cent respectively. The standard deviation in the azimuth of 4.28° in Fig. 8(b) is reduced by 25, 24 and 20 per cent respectively, if the different sediment wedges are taken into account.

That the models used are still too simple can be seen in Fig. 9, where the arrows with full heads are the mislocation vectors (data) in each bin. The three arrows with open heads are the data after the removal of the contribution of

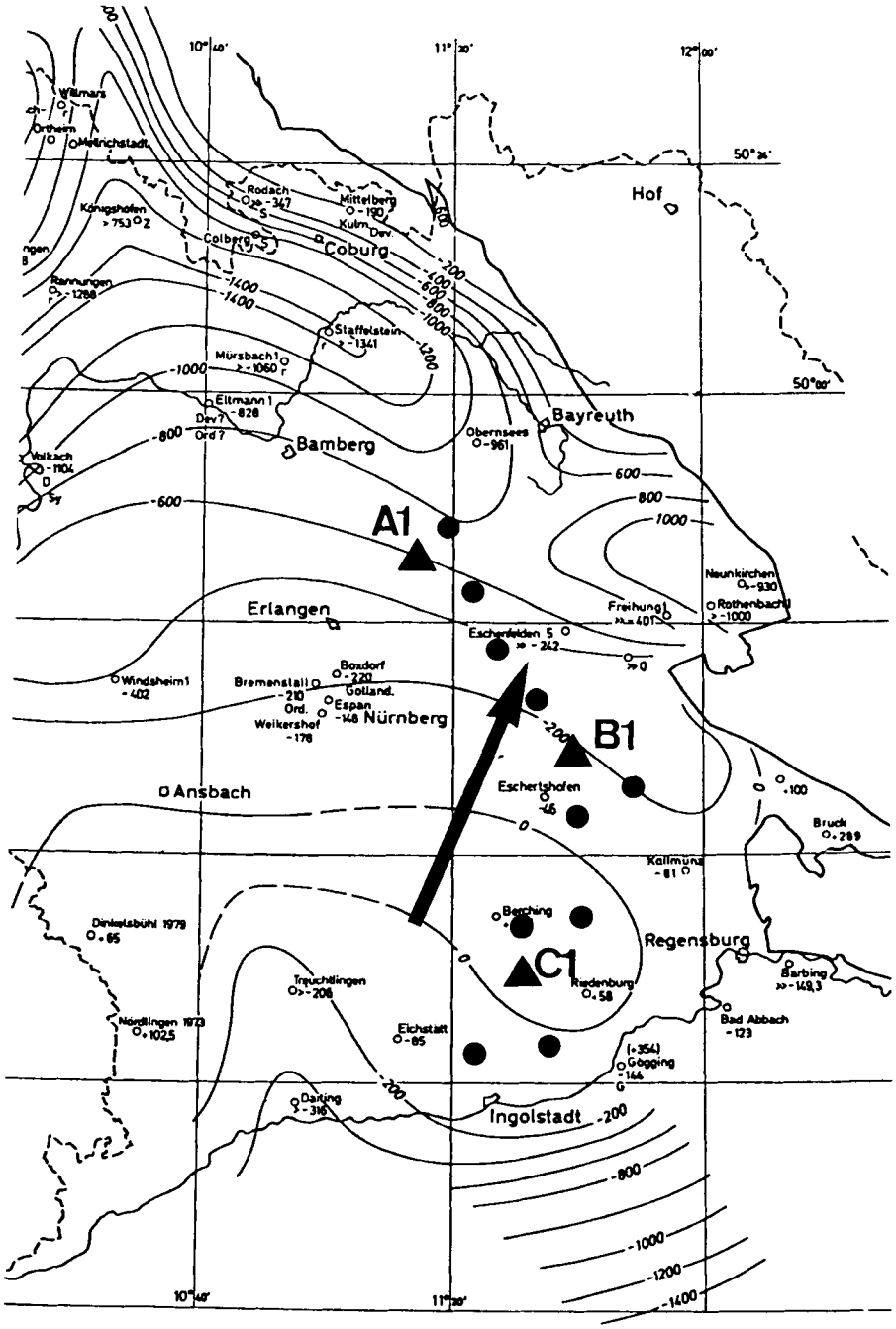

Figure 5. Contour map of the top of the basement under the GRF array (see also Fig. 1) with respect to *sea-level* modified after Gudden & Schmid (1985). The arrow indicates the direction of the dip of the sedimentary wedge. The elevation at A1, B1 and C1 is 499, 494 and 512 m above sea-level respectively.

the sedimentary wedge models. If a certain sedimentary wedge would be solely responsible for the mislocation vector, the length of the arrow with open head would shrink to zero. As can be seen in Fig. 9, a remarkable reduction of the size of the mislocation vectors can be achieved with the three models except for bins 5 and 6.

This mismatch in those two bins is possibly due to local effects like the Dinkelsbühl–Berching high of the basement under the southern part of the array (see Fig. 5) and the fact that the major fault systems strike in the SE direction (see Fig. 1).

The three models give relative traveltime residuals of 0.2, 0.25 and 0.3 s between station A1 and C1 respectively, i.e. about 40 to 60 per cent of the *average* residual documented by Faber *et al.* (1986, see fig. 7 there).

Since it is possible to explain the observed traveltime residuals to a large extent by the effect of the sedimentary wedge, the need to postulate crustal and lithospheric inhomogeneities of the size and strength derived by Faber *et al.* (1986) is reduced.

As shown in Fig. 9 we are not able to explain all details of the mislocation vectors with such simple, first-order models,

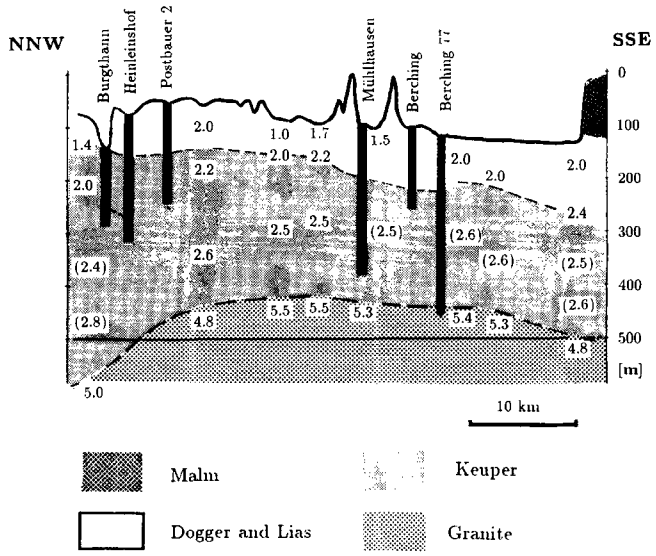

Figure 6. *P*-wave velocities derived from the refraction survey along a profile from a point near C1 to NNW (see Fig. 1) modified after Bader (1982b). The Dogger, Lias and Keuper in particular (loosely connected sandstones and clay or shale) have very low *P*-wave velocities. Vertical solid bars indicate boreholes.

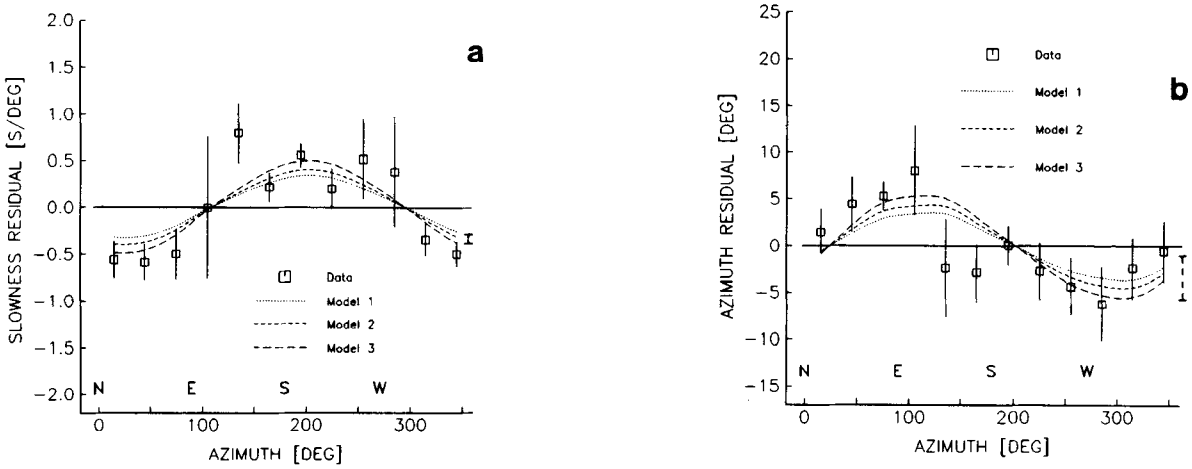

Figure 7. (a) Average values of slowness residuals in 30° bins for the data and the three models. The vertical bars at the data are the standard deviations in the bins. The maximum standard deviation occurring in the *models* is indicated at the right of the model curves. (b) As (a) but for the azimuth residuals.

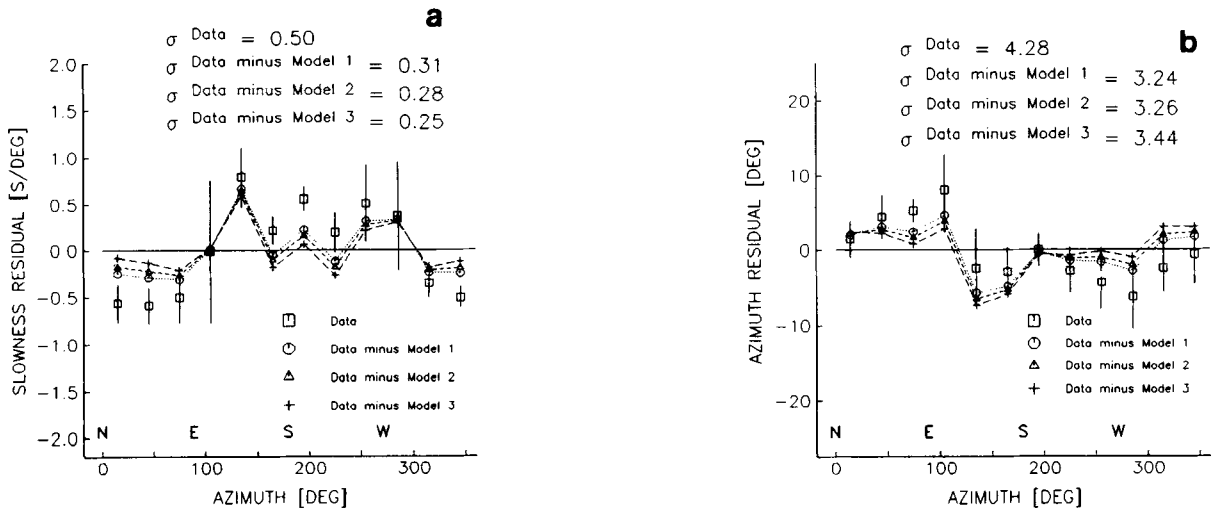

Figure 8. (a) Average values of slowness residuals in 30° bins. Data and data after the removal of the contribution of the sedimentary wedge for the three models. The standard deviation (σ) of the values shown, i.e. the deviation from a horizontally layered medium, is also given. Taking into account the different models reduces the standard deviation by 38, 44 and 50 per cent respectively. (b) As (a) but for the azimuth residuals. The standard deviation is reduced by 25, 24 and 20 per cent respectively.

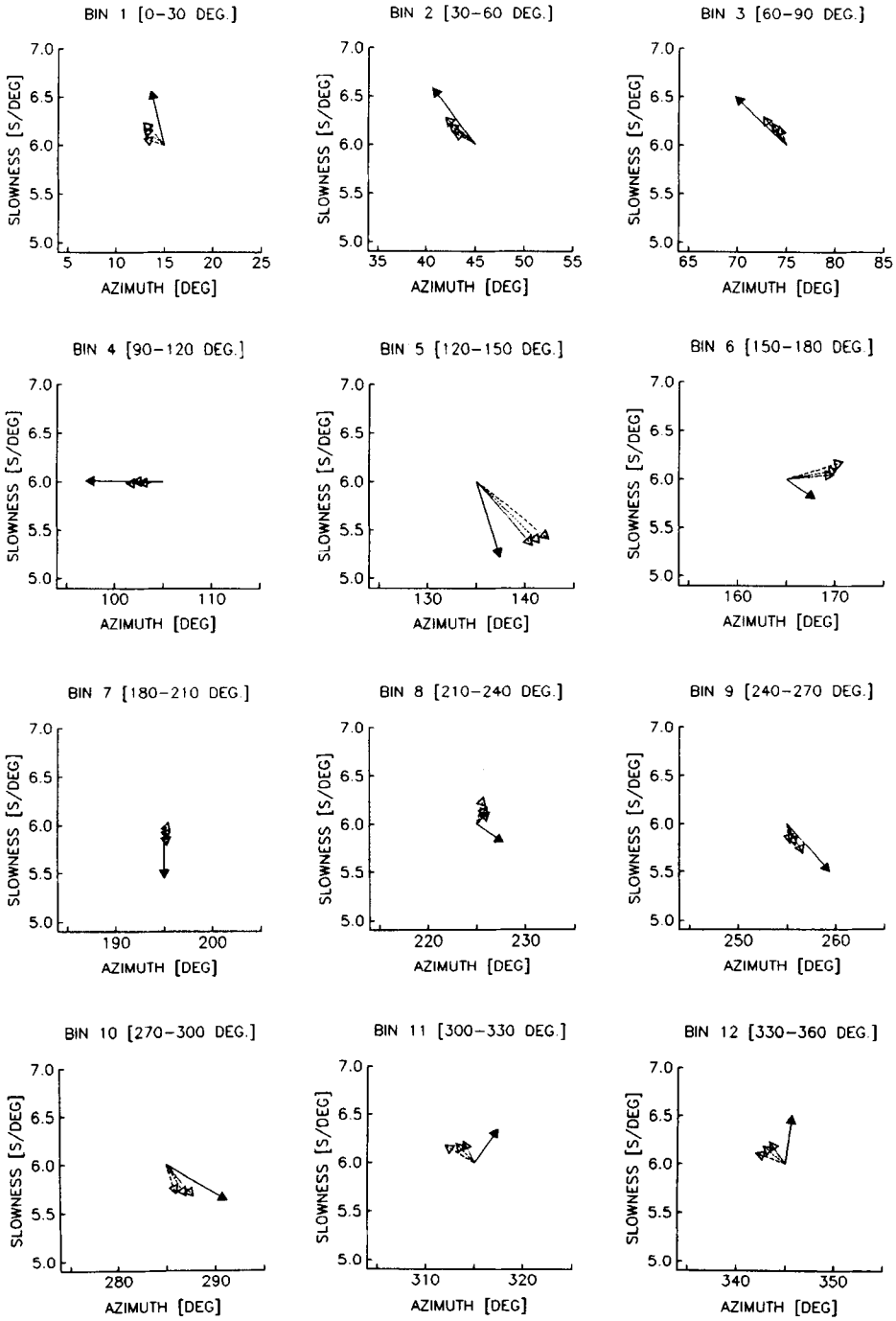

Figure 9. Average of the mislocation vectors in 30° bins. The tails of the vectors are placed at the centre of the bin. Data are the arrows with full heads. Data minus the effects of the models 1, 2 and 3 are the arrows with open heads and short dashed, medium dashed and long dashed shafts respectively; see also Figs 8(a) and (b).

but would like to point out that the principal features, i.e. the *pattern*, of the mislocation vectors and about half of the amplitude of the effects observed can be reproduced by models derived from geological evidence, borehole measurements and refraction surveys.

The effect of such a sedimentary wedge on the amplitudes and the waveforms of recordings from teleseismic events will be the topic of future work.

CONCLUSIONS

We study the influence of a sedimentary wedge on the mislocation vectors of the GRF array. Using the information obtained from local geology, refraction surveys and borehole measurements, first-order models for the sediments under the GRF array are presented.

The models consist of a sedimentary wedge dipping NNE

with about 0.8° dip. The P velocity in the sediments is between 2.2 and 2.4 km s^{-1} and in the granite basement between 5.6 and 5.8 km s^{-1}. Such models are able to produce to a large extent the slowness–azimuth mislocation *pattern* observed at the GRF array and a major part of the relative traveltime residuals observed.

This demonstrates the importance of removing the effects of the sedimentary cover before tomographic inversions are applied.

ACKNOWLEDGMENTS

We are grateful for stimulating discussions with S. Faber and D. Seidl and for their contribution in establishing the database our work is based on. We would also like to thank H. Aichele, G. Müller, R. Kind, J. Schweitzer and two anonymous reviewers for helpful comments on this paper and K. Bader, H. Gudden, B. Schröder and A. Stein for their comments on the geology in the area of the GRF array. One of us (MW) was supported by a grant of the Deutsche Forschungsgemeinschaft (DFG). The Gräfenberg array is operated by the Bundesanstalt für Geowissenschaften und Rohstoffe (BGR) and funded by the DFG.

REFERENCES

Bader, K., 1982a. Die seismischen Geschwindigkeiten bis zum Grundgebirge bei der Forschungsbohrung Dinkelsbühl 1001, *Geologica Bav.*, **83**, 87–88.

Bader, K., 1982b. Die Grundgebirgstiefe längs eines Profils von Burgthann bis Beilngries aufgrund refraktionsseismischer Messungen, *Geologica Bav.*, **83**, 123–127.

Berteussen, K. A., 1976. The origin of slowness and azimuth anomalies at large arrays, *Bull. seism. Soc. Am.*, **66**, 719–741.

Faber, S., Plomerova, J. & Babuška, V., 1986. Deep seated lateral velocity variations beneath the GRF-Array inferred from mislocation patterns and P residuals, *J. Geophys.*, **60**, 139–148.

Gudden, H., 1970. Stratigraphische Gliederung einiger Tiefbohrprofile in die höhere Trias unter der nördlichen Frankenalb anhand bohrlochphysikalischer Messungen (Tiefbohrungen Eschenfelden B1 und B2), *Geol. Bl. NO-Bayern*, **20**, 105–119.

Gudden, H., 1982. Die Forschungsbohrung Berching 1977, Konzeption, Ablauf und Deutung der Ergebnisse, *Geologica Bav.*, **83**, 95–112.

Gudden, H. & Schmid, H., 1985. Die Forschungsbohrung Obernsees—Konzeption, Durchführung und Untersuchung der Metallführung, *Geologica Bav.*, **88**, 5–21.

Harjes, H. P. & Hanka, W., 1986. The contribution of broadband array seismology to seismic monitoring of underground nuclear explosions, *Geol. Jahrbuch, Reihe E*, **35**, 105–120.

Jeffreys, H. & Bullen, K. E., 1940. *Seismological Tables*, British Association for the Advancement of Science, Burlington House, London.

Salger, M. & Schmid, H., 1982. Die Forschungsbohrung Eschertshofen 1981 (Vorläufige Mitteilung), *Geologica Bav.*, **83**, 145–161.

Schmid, H., 1982. Die Forschungsbohrung Kallmünz, (Kurzmitteilung), *Geologica Bav.*, **83**, 163–165.

Schmidt-Kaler, H., 1969. Keuper und Jura in der Tiefbohrung Riedenburg, *Geol. Bl. NO-Bayern*, **19**, 97–112.

Schmidt-Kaler, H., 1985. Das geologische Profil der Thermalwasserbohrung Bad Abbach südlich Regensburg (Grundgebirge bis Kreide): Stratigraphische Gliederung und paläogeographische Folgerungen, *Geol. Bl. NO-Bayern*, **34/35**, 273–302.